Nanoscale

PAPER

Cite this: *Nanoscale*, 2015, **7**, 15789

Functional nicotinic acetylcholine receptor reconstitution in Au(111)-supported thiolipid monolayers

Diego E. Pissinis,†[a] Carolina Diaz,†[a] Eliana Maza,[a] Ida C. Bonini,[b] Francisco J. Barrantes,[c] Roberto C. Salvarezza[a] and Patricia L. Schilardi*[a]

Received 20th June 2015,
Accepted 21st August 2015

DOI: 10.1039/c5nr04109k

www.rsc.org/nanoscale

The insertion and function of the muscle-type nicotinic acetylcholine receptor (nAChR) in Au(111)-supported thiolipid self-assembled monolayers have been studied by atomic force microscopy (AFM), surface plasmon resonance (SPR), and electrochemical techniques. It was possible for the first time to resolve the supramolecular arrangement of the protein spontaneously inserted in a thiolipid monolayer in an aqueous solution. Geometric supramolecular arrays of nAChRs were observed, most commonly in a triangular form compatible with three nAChR dimers of ~20 nm each. Addition of the full agonist carbamoylcholine activated and opened the nAChR ion channel, as revealed by the increase in capacitance relative to that of the nAChR–thiolipid system under basal conditions. Thus, the self-assembled system appears to be a viable biomimetic model to measure ionic conductance mediated by ion-gated ion channels under different experimental conditions, with potential applications in biotechnology and pharmacology.

Introduction

Solid supported membranes have been used as model systems to study the surface chemistry of cells.[1] Membrane proteins attached to or embedded in the lipid bilayer of the cells exhibit a wide range of functions such as cell-surface recognition, signal transduction and substance transport across the membrane.[2] The successful reconstitution of function in artificial biomimetic systems is an important requisite for characterizing the properties of cell-surface receptors and physiologically relevant membrane proteins, and it constitutes an essential step in establishing the potential use of the reconstituted system as a diagnostic biosensing assay with biotechnological and pharmacological applications.[3]

The preparation of protein-artificial membrane systems for biosensing applications can proceed *via* a bottom-up approach, *i.e.* by self-assembly of the membrane components and proteins on a solid conducting substrate.[4] Self-assembled thiol monolayers on Au(111) have been extensively used as suitable environments for anchoring different types of biomolecules to Au surfaces while preserving their biological properties.[5] In particular, different types of thiolipids have been developed to create membrane mimetic surfaces capable of anchoring membrane proteins.[6–11] The strong covalent thiol–Au bond provides a robust link to the metal platform, while the external lipids facilitate the adsorption of peripheral membrane proteins and the insertion of the membrane-embedded proteins. The structure and function of the complex supramolecular system require a complete characterization at the nanometer level in aqueous environments. The rigid thiolipid self-assembled monolayer (SAM) decreases protein lateral displacement and therefore facilitates the imaging of monomers and oligomers of membrane proteins in aqueous solutions by atomic force microscopy.[12] Furthermore, high quality thiolipid self-assembled monolayers exhibit excellent blocking properties, thus allowing the detection of small changes in ionic currents induced by conformational changes in the membrane proteins, a requisite for amperometric biosensors.

nAChR is a membrane protein belonging to the superfamily of pentameric ligand-gated ion channels.[13] From a structural point of view, the monomeric glycoprotein macromolecule is a cylinder roughly 16 nm in length and 8 nm in diameter, with an average MW of 290 kDa, and it is composed of five pseudo-symmetrically arranged petal-like subunits surrounding a central ion pore.[14] Each subunit possesses four transmembrane (TM) domains with both the N- and C-termini located

[a]*Instituto de Investigaciones Fisicoquímicas Teóricas y Aplicadas (INIFTA), CONICET – Departamento de Química, Facultad de Ciencias Exactas, Universidad Nacional de La Plata, CC16, Suc. 4, La Plata, Buenos Aires, Argentina.*
E-mail: pls@inifta.unlp.edu.ar, pls@quimica.unlp.edu.ar; Fax: +54 221 4254642; Tel: +54 221 4257430/7291
[b]*Instituto de Investigaciones Bioquímicas de Bahía Blanca (INIBIBB), 8000 Bahía Blanca, Buenos Aires, Argentina*
[c]*Laboratory of Molecular Neurobiology, BIOMED, UCA-CONICET, Faculty of Medical Sciences, Av. Alicia Moreau de Justo 1600, 1107 Buenos Aires, Argentina*
†These authors contributed equally.

extracellularly. The four TM domains, consisting of approximately 20 amino acid residues each, are arranged in the form of three concentric rings;[15,16] the inner ring is made up of five TM2 segments lining the walls of the pore that provides an ion pathway across the post-synaptic membrane. TM1 and TM3, which comprise the intermediate ring, are partly exposed to membrane lipids, and the outer ring, formed exclusively by five TM4 domains, is totally immersed in the membrane lipids. TM4 has been postulated to convey the influence of the lipid microenvironment to the rest of the nAChR macromolecule.[15] The receptor complex binds two molecules of acetylcholine at the interface of the two alpha subunits with non-alpha subunits, leading to the opening of the pore by a mechanism that possibly involves the twisting and rotation of all the TM2 helices.[17,18] The cation specificity of nAChR is related to the negatively charged rings of the amino acid side chains located at the cytoplasmic end of the receptor ion pore and helps to remove the hydration shell formed by ions in an aqueous solution. The hydrophobic region located within the pore lumen, formed by valine and leucine residues, constitutes the region wherein the dehydrated ions cross the pore, and hence constitutes the ion selectivity region.[19]

There have been previous successful attempts to reconstitute the nAChR protein in lipid bilayers[20–22] and to study some of its properties with atomic force microscopy (AFM);[23–26] however, to the best of our knowledge, there are no studies using these approaches that have resulted in the successful immobilization of the receptor protein on an Au-supported substrate, offering biomimetic analytical capabilities.

In this study, nAChR incorporated into an Au-supported thiolipid self-assembled monolayer (SAM) was studied using a combination of AFM, SPR, Fourier transform infrared spectroscopy (FTIR) and electrochemical techniques. We used succinic acid-2-(thioglycolic acid-[tetraethylene glycol ester-[D,L-α lipoic acid ester]])-1,4-bis(heptacosa-10,12-diynyl)-ester, denoted henceforth as the thiolipid, to form a densely packed SAM linked by two S–Au bonds per molecule to ultraflat preferred oriented Au(111) substrates. The tether/spacer molecules provide a hydrophilic layer between the lipid and the gold substrate, establishing a water-containing space, which reduces the influence of the metal surface, preventing denaturation of the transmembrane proteins.[27] We show that this thiolipid–Au platform provides a suitable environment for anchoring the nAChR protein, allowing *in situ* imaging of the protein arrangement at the molecular level in an aqueous solution for the first time. The ion transport blocking ability of the thiolipid SAM also allowed us to measure the changes in capacitance induced by a typical nAChR full agonist, carbamoylcholine (Carb), thus verifying the preservation of function of the macromolecule under these experimental conditions.

Results and discussion

In this work, a detailed study of the insertion of nAChR into a thiolipid SAM on Au(111) using a multitechnique approach is presented. We start with the characterization of the thiolipid SAM, followed by insertion of the protein into the lipid environment and finally, the demonstration of ion transport through the reconstituted protein–thiolipid system. This study is at the cross section of biophysics and physical chemistry, with the aim of developing biomimetic and biosensing platforms.

Self-assembly of the thiolipid SAM on Au(111)

The thiolipid surface coverage (θ) on the Au surface can be estimated by measuring the charge density (q) involved in the reductive desorption peak, whereas the peak potential value (E_p) of the thiolipid SAM is indicative of the stability of the SAM (Fig. 1a).[28] After 24 h of immersion of the Au substrate in the thiolipid-containing solution, the reductive desorption yielded $E_p = -1.19$ V and $q = 63.7 \pm 0.4$ μC cm^{-2}, a value slightly smaller than that found for alkanethiols adsorbed on the same substrate in a standing up configuration ($q = 75$ μC cm^{-2}, $\theta = 0.33°$, surface excess $\Gamma_t = 7.6 \times 10^{-10}$ mol cm^{-2}, and molecular area $A = 21$ Å^2).[29] However, considering that each thiolipid molecule contains S atoms that form two thiolate bonds, the electrodesorption process involves two electrons per thiolipid molecule. Therefore, the surface coverage of the thiolipid results in $\theta = 0.14°$ (surface excess $\Gamma_t = 3.2 \times 10^{-10}$ mol cm^{-2}, molecular area $A = 50$ Å^2). As expected, θ decreases slightly and E_p moves in the positive direction for shorter immersion times (Fig. 1b). However, it is known that the reductive desorption method could overestimate the surface coverage of thiols on the Au(111) surface by about 20%.[30]

We also tested the blocking ability of the thiolipid layer toward ionic and water transport by analyzing the electrical double layer of the clean Au and the same substrate after SAM formation by cyclic voltammetry (Fig. 1c). It is evident that the thiolipid layer forms a dense and hydrophobic layer, drastically reducing the electrical double layer of Au.

AFM imaging of the thiolipid SAM taken in a Triton X-100 aqueous solution revealed a disordered structure formed by agglomerates 8 to 10 nm in size (Fig. 2a and inset), consistent with a liquid-crystalline phase of the terminal hydrocarbon chains.[29] In fact, the FTIR spectrum of the thiolipid SAM on the Au substrate (Fig. 1d) showed two main peaks at 2918 cm^{-1} and 2851 cm^{-1}, corresponding to the asymmetric and symmetric CH_2 stretching, respectively.[31] The position of the asymmetric CH_2 maxima is an indication for the conformational order of the alkyl chains.[32,33] In fact, totally disordered alkyl chains exhibit the CH_2 stretching band at values found for liquid alkanes (2924 cm^{-1}), whereas for crystalline alkanes, a value of 2915 cm^{-1} is reported.[34] In the case of self-assembled monolayers, frequencies lower than 2920 cm^{-1} are characteristic of well ordered adlayers with alkyl chains in all-*trans* conformations, whereas higher frequencies indicate the presence of *gauche* defects and less ordered chains.[35] The thiolipid SAM thickness (h) in the liquid environment was estimated by opening a window by repetitive AFM tip scanning, resulting in $h = 5.25 \pm 0.66$ nm (Fig. 2b), a figure close to that expected for this molecule (Fig. 2c).

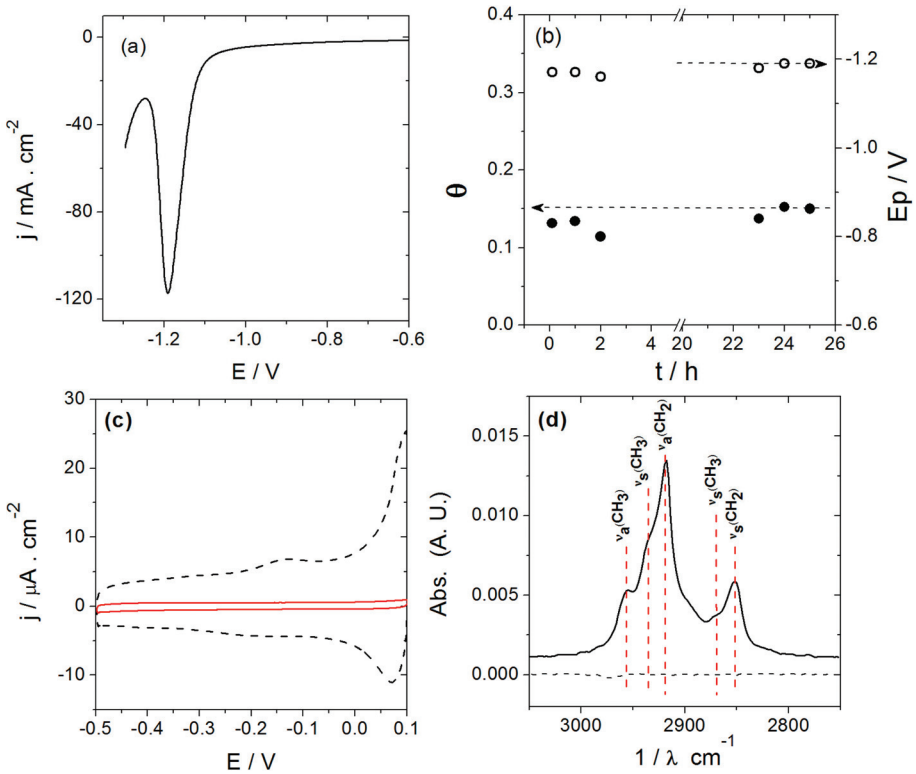

Fig. 1 (a) Current density (j) *vs.* potential (E) profile for the reductive desorption of the thiolipid SAM on Au prepared by immersion of the substrate for 24 h in solution containing the thiolipid. Electrolyte: 0.1 M NaOH, scan rate: 0.1 V s^{-1}. (b) Coverage (θ) (left axis) and E_p (right axis) *vs.* immersion time of the Au substrate in the thiolipid-containing solution. (c) Cyclic voltammogram showing the double layer potential region of Au(111) (dashed line) and the thiolipid SAM-covered Au (red solid line). Electrolyte: 0.1 M NaOH, scan rate: 0.1 V s^{-1}. (d) FTIR absorption spectrum of the thiolipid SAM on Au.

nAChR incorporation into the thiolipid SAM

The self-assembled thiolipid SAM was studied *via* SPR for its ability to incorporate the nAChR protein. Thus, the thiolipid SAM was first formed *ex situ* on the SPR sensor surface, followed by *in situ* evaluation of the protein adsorption. Fig. 3a and b show the SPR curves of the Au–thiolipid and Au–thiolipid–protein surfaces. The sensorgrams revealed that both molecules have fast adsorption kinetics on the substrate, reaching saturation for adsorption times $t > 30$ min. After the weakly adsorbed thiolipid and proteins were removed by flowing a buffer dissolution, final changes of $\Delta\theta = 0.14°$ and 0.03° were obtained for the thiolipid and protein, respectively.

These data were subsequently used to calculate the surface excess of the thiolipid (Γ_t) and protein (Γ_p) using eqn (1), resulting in $\Gamma_t = 148$ ng cm^{-2} ($\Gamma_t = 1.5 \times 10^{-10}$ mol cm^{-2}, MW = 1312 g mol^{-1}) and $\Gamma_p = 31.2$ ng cm^{-2} ($\Gamma_p = 1.0 \times 10^{-13}$ mol cm^{-2}, MW = 290 kDa), a figure that implies ~600 monomers μm^{-2}. As expected, the adsorption of the protein on the Au substrate without the thiolipid molecular layer leads to higher values ($\Gamma_p = 52$ ng cm^{-2}).[36] In fact, it is well known that significant protein aggregation and unfolding due to strong interactions with the high-energy gold surface[11] occur when proteins are directly adsorbed on gold. It is also interesting to compare the thiolipid surface concentration derived from the reductive desorption measurements with those obtained from the SPR technique. The reductive desorption technique, for θ values estimated for immersion times <2 h (Fig. 1b), results in $\Gamma_t = 2.7 \times 10^{-10}$ mol cm^{-2}, a figure somewhat larger than the value of $\Gamma_t = 1.5 \times 10^{-10}$ mol cm^{-2} that was obtained from the SPR measurements. The difference can be explained by considering that reductive desorption method overestimates the surface coverage of thiols on Au(111) by 20%[30] and that thiolipid adsorption in the SPR measurements is made on polycrystalline Au rather than Au(111).

Evidence of protein adsorption on the thiolipid SAM was also obtained by FTIR-ATR (Fig. 4), wherein the characteristic bands related to the protein amide I groups appear in the 1620 and 1650 cm^{-1} regions.[37] The typical bands at 1740 cm^{-1}, corresponding to the carbonyl stretching band of the thiolipid,[11,37] and at 1511 cm^{-1}, corresponding to the bending vibration of the OH group assigned to Triton X-100,[38] are also clearly visible in the spectra.

We used AFM-tapping in the Triton X-100 environment to study the structure of the nAChR on the Au supported thiolipid SAM. Fig. 5a shows a typical topographic AFM image of the sample. The image depicts nanometer-sized oligomers formed by smaller elements that randomly cover the thiolipid–Au

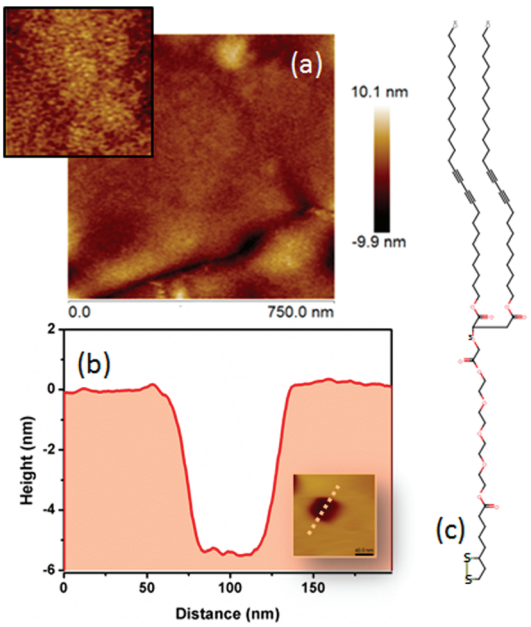

Fig. 2 (a) AFM image (750 × 750 nm^2) of the thiolipid SAM in a liquid environment (Triton X-100 aqueous solution) on the Au substrate. The inset (125 × 125 nm^2) shows a detail of the thiolipid covered Au substrate. (b) Cross section analysis of a window opened by repetitive tip scanning, showing the thickness of the SAM. (c) Molecular structure of the thiolipid (succinic acid-2-(thioglycolic acid-[tetraethylene glycol ester-[D,L-α lipoic acid ester]])-1,4-bis(heptacosa-10,12-diynyl)-ester).

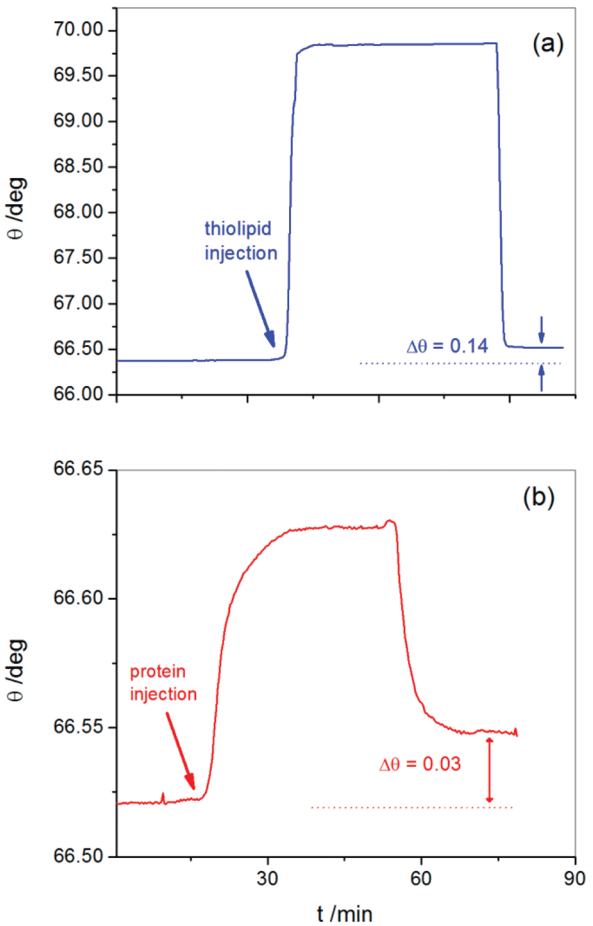

Fig. 3 SPR curves of the thiolipid on Au(111) and nAChR on the thiolipid–Au(111) surfaces.

surface. Most of these oligomers adopt a triangular shape (56.4%) (Fig. 5b), although square-shaped bodies (10.3%), trapezoidal bodies (12.8%), linear chains (7.7 5%) and isolated units (12.8%) were also observed in the images, indicating that the triangles are not tip-induced artifacts (Fig. 5a). The cross-section analysis (Fig. 5c) of the oligomers reveals that the smaller elements are ~20 nm in size, a figure consistent with dimers of the individual 290 kDa monomeric nAChR protein (19 nm[39]), after taking into account the tip-size effects. It can be noted that the oligomers form a supramolecular arrangement consisting of three grouped dimers (red circle in Fig. 5b). The triangular shaped structures are 70 to 100 nm in size, thus closely resembling the 70 nm nanoclusters of muscle-type nAChR resolved by STED super-resolution optical microscopy in Chinese hamster ovary cells.[40] Dimers have also been reported to be predominant structures from TEM imaging of uranyl acetate negatively-stained nAChRs.[39] Interestingly, trimers similar to those constituting the predominant species in the present study have also been imaged in the case of the major outer-membrane porin OmpF from *Escherichia coli*.[12] Our results differ from previously reported data for this protein embedded in lipid bilayers supported on mica, wherein monomers seem to be the major species observed.[24] This apparent discrepancy can be explained by differences in the redox states of the samples.[39]

Statistical analysis of the number of the smallest elements present in the AFM images gives ~250 μm^{-2}. Assuming that

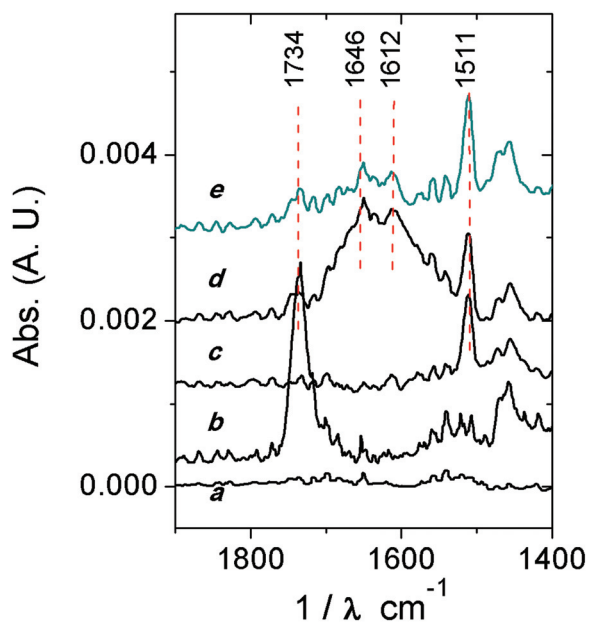

Fig. 4 FTIR spectra of (a) Au substrate; (b) thiolipid on Au (drop casting); (c) Triton X-100 on Au (drop casting); (d) nAChR on Au (drop casting); (e) nAChR incorporated into the thiolipid SAM (as described in the Experimental section).

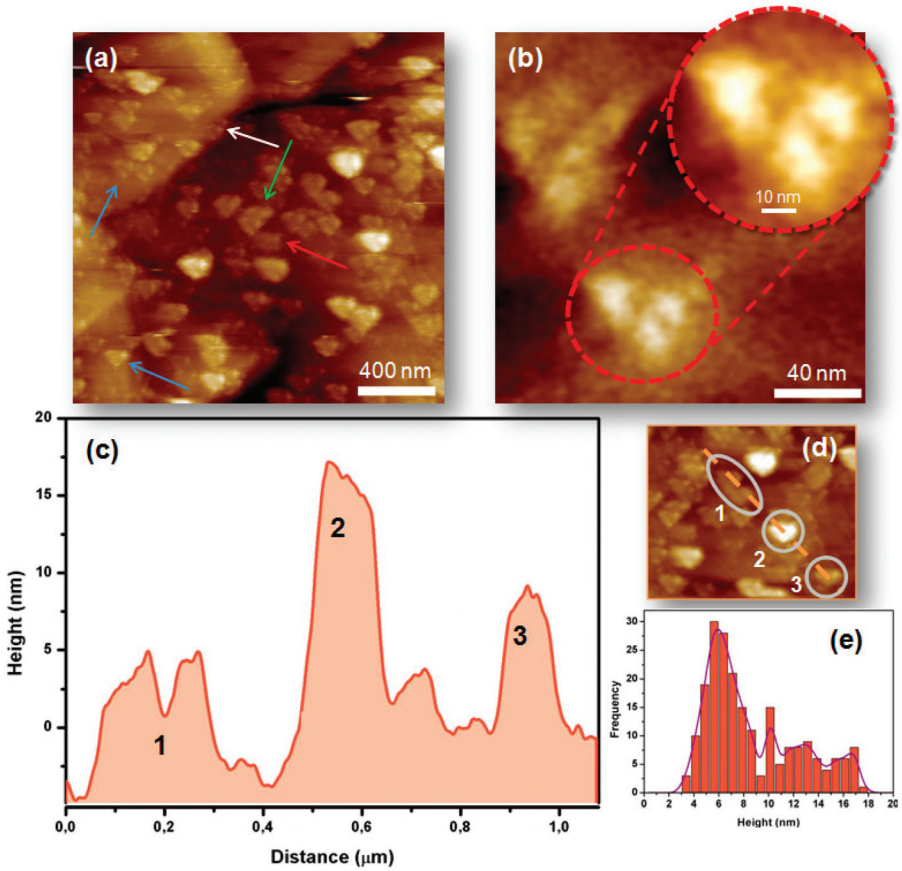

Fig. 5 (a) AFM-tapping in liquid for the nAChR on Au-supported thiolipid SAM; (b) detail of the image in (a) showing the different oligomeric arrangements of the macromolecules. Different shaped oligomers in (a) are indicated by arrows. Light blue: triangular; red: square; green: trapezoidal; white: linear. (c) Cross-section of image (d); (e) histogram showing the heights of the nAChR assemblies in relation to the thiolipid-SAM surface.

these features are dimers, this results in ~500 μm^{-2} monomers, which is in reasonable agreement with the values estimated by SPR data.

The histogram in Fig. 5c reveals that 45% of the dimers are 5 to 8 nm in height (Fig. 5c, histogram), indicating that an important fraction of the protein is most likely inserted in the thiolipid layer. Although it is known that nAChR protrudes ~8 nm from the lipid extracellular hemilayer, slightly smaller values are also consistent with inserted proteins, considering that the measured height can be influenced by the force exerted by the AFM tip. The disordered liquid-crystalline state of the outer lipid layer (see Fig. 1d) should facilitate protein incorporation into the thiolipid SAM. Note that other important fractions of protein oligomers (40%) are greater than 8 nm (Fig. 5c, histogram), suggesting that they are either partially incorporated or simply adsorbed on the thiolipid SAM.

The functionality of the inserted nAChR protein was estimated by measuring the double layer current density (j) response of the nAChR–thiolipid SAM-Au at $E = -0.2$ V after the addition of Carb, a full nicotinic agonist that binds and activates the nAChR (Fig. 6).

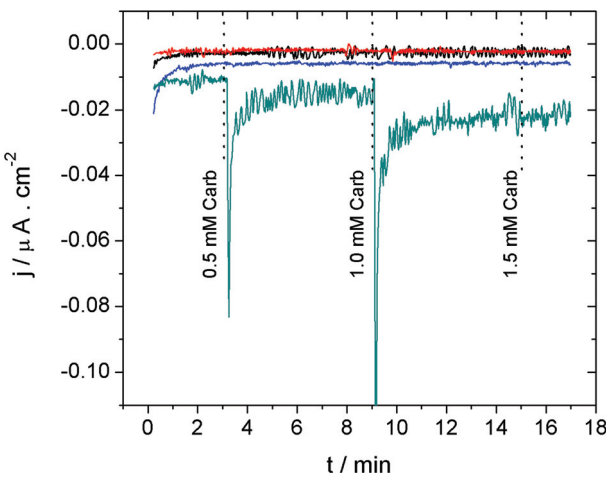

Fig. 6 Current density (j) *vs.* time for thiolipid SAM-Au (black), thiolipid SAM-Au with addition of Carb at 3, 9 and 15 min (red), nAChR–thiolipid SAM-Au (blue), nAChR–thiolipid SAM-Au after addition of Carb to reach final concentrations of 0.5 mM (3 min), 1 mM (9 min) and 1.5 mM (15 min) (green). Electrolyte: 0.1 M NaOH, $E = -0.2$ V, rotation speed: 300 rpm.

The sudden increase in current density after the addition of Carb at 3 min (final concentration: 0.5 mM) and 9 min (final concentration: 1 mM) to the nAChR–thiolipid SAM-Au system indicates pore opening and ion transport through the thiolipid SAM, thus increasing the capacitance of the Au substrate. However, further addition (final concentration: 1.5 mM, 15 min) of the agonist did not produce noticeable changes in the current density, indicating that ionic transport through the channel achieved a steady state at 1 mM concentration. Note that similar experiments for the thiolipid–Au system (Fig. 6) show no response after Carb addition, thus indicating that the protein is responsible for the changes in double layer current density.

Finally, to test if the ligand-mediated activation was sustained over time, the Carb treated nAChR–thiolipid SAM-Au sample was transferred to an electrochemical cell to carry out voltammetric runs in the double layer potential (Fig. 7). In all cases, a clear increase in the capacitance was observed, indicating activation of the nAChR receptors by the agonist. This increase in capacitance persisted during cycling times, suggesting that the protein remained active after repetitive potential cycling. It was noticed that no effects on the double layer capacitance are observed after the addition of Triton X-100 to the thiolipid SAM (Fig. 7b). Therefore, no damage of the SAM is produced by the presence of this molecule, in agreement with previous work in similar systems,[41] since the thiolipid layer is densely packed and strongly bonded to the Au surface by the S head.

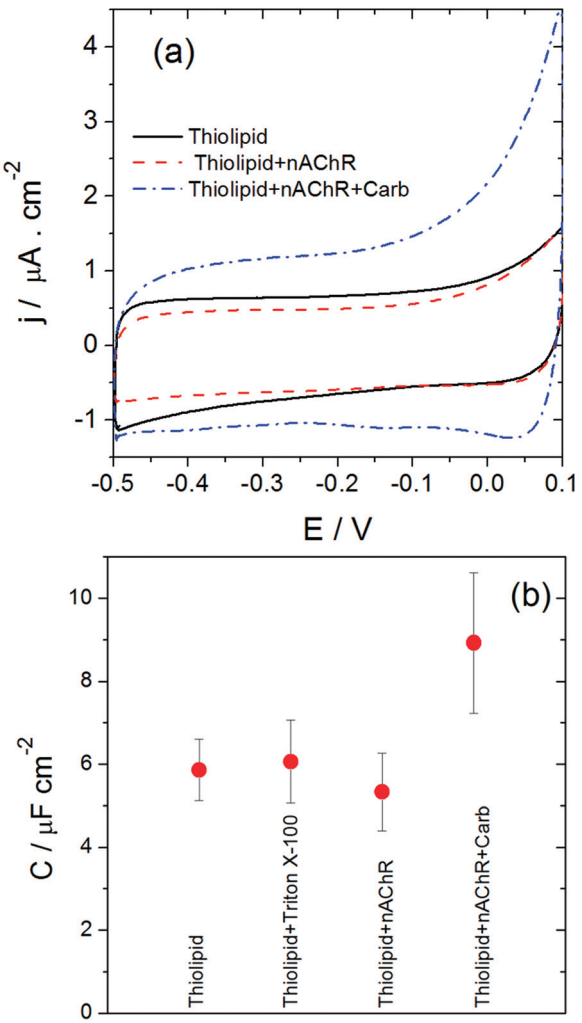

Fig. 7 (a) Current density (j) *vs.* potential (E) profiles for thiolipid SAM-Au (black), nAChR–thiolipid SAM-Au (red) and nAChR–thiolipid SAM-Au after addition of Carb to reach a 1 mM final concentration (blue); electrolyte: 0.1 M NaOH; sweep rate: 0.1 V s^{-1}. (b) Double layer capacitance at −0.2 V calculated from data in (a).

It can be noted that the incorporation of other molecules inside SAM defects is usually the reason for improved ion transport and changes of capacitance. The results in Fig. 6 and 7 allow us to discard this possibility. First, the electrochemical data indicate that the double layer capacitance of the thiolipid-modified Au substrate does not change after the addition of Triton X-100 (Fig. 7b). Second, after addition of the protein in Triton X-100 solution, the capacitance is reduced with respect to that found for the thiolipid SAM alone (Fig. 7). Note that the addition of Carb to the thiolipid SAM-covered Au substrate does not induce any current increase (Fig. 6). Therefore, the enhanced ion transport cannot be related to the incorporation of these molecules in the thiolipid SAM.

Finally, we analyzed the ion current for this self-assembled platform. Assuming that the conductance of a single channel is ~14–33 pS[42] and that the number of inserted monomers is 10^{10} cm^{-2}, as derived from the SPR and AFM data, the current increase of about 0.5 μA cm^{-2} (Fig. 7a) implies that ~10^5 channels are opened after Carb addition. In fact, this increase in current would be higher if the basal current for the assembled system was decreased, for instance, by the fusion of small unilamellar vesicles to complete a bilayer.[43]

Conclusions

Ion-channel based biosensors with high sensitivity and selectivity are becoming increasingly important in areas such as health care, drug screening and environmental control.[44] The need to preserve the function of these ion-channel proteins makes it indispensable to build strong and stable lipid platforms, wherein the protein can be incorporated. In this study, we show that nAChR, an archetypal transmembrane protein that mediates ion transport in excitable membranes, has been successfully integrated into a thiolipid SAM on a gold substrate. The supramolecular arrangement and oligomeric structure of the incorporated protein have been resolved for the first time in an aqueous environment. From the shape and size of the arrays observed by AFM, nAChR appears to consist of dimers inserted in the thiolipid layer. Most importantly, the functionality of nAChR is preserved upon insertion in the thiolipid SAM, as indicated by the increase in conductivity after addition of the full agonist Carb.

Experimental

Reagents

Thiolipid (succinic acid-2-(thioglycolic acid-[tetraethylene glycol ester-[D,L-α lipoic acid ester]])-1,4-bis(heptacosa-10,12-diynyl)-ester), denoted henceforth as thiolipid, was kindly provided by Prof. Helmut Rinsgdorf from the University of Mainz.

nAChR purification

nAChR protein was purified from *T. californica* electric tissue as described previously.[39] Briefly, frozen *Torpedo californica* (Aquatic Res. Consultants, San Pedro, CA) electric tissue was chopped into small pieces and homogenized using a Virtis homogenizer; the homogenate was centrifuged for 2 h at 40 000*g* and 4 °C, resulting in a pellet of crude membranes. The membranes were then solubilized in 1% sodium cholate (2 mg ml^{-1} protein concentration) for 45 min at 4 °C and centrifuged at 74 000*g* for 1 h to discard the insoluble material. The detergent-soluble material was then subjected to affinity chromatography. The affinity column was prepared by coupling cystamine to Affi-Gel 10, reduction with dithiothreitol, and a final coupling step with bromoacetylcholine bromide. The column was then washed several times with dialysis buffer (100 mM NaCl, 0.1 mM phosphate, 0.1 mM EDTA, 0.02% NaN_3, pH 7.8) containing 1% sodium cholate. The nAChR protein was finally eluted from the column with 250 mM NaCl, 0.1 mM EDTA, 0.02% NaN_3, 5 mM phosphate, pH 7.8, containing 0.5% cholate and 10 mM Carb. After elution from the column, nAChR was dialyzed against 1 L of dialysis buffer with five buffer changes (every 12 h) at 4 °C. The purity of the nAChR protein was verified by SDS-PAGE, and the protein concentration was determined by the method of Lowry.[45] The samples were stored at −70 °C until use.

Sample preparation

Thiolipid monolayer. The gold substrates consisted of a thin layer of gold deposited on glass and were purchased from Arrandee® (Germany). The substrates were sonicated in absolute ethanol and annealed in a butane flame to obtain (111) terraces. The substrates were then immersed in a 0.1 mg mL^{-1} thiolipid ethanolic solution for 24 h, gently rinsed three times with absolute ethanol and dried in air.

nAChR immobilization. A 30 μl drop of the nAChR solution (0.1 mg ml^{-1} in 0.1% v/v Triton X-100 aqueous solution) was poured onto the thiolipid-modified surface; after 1 h of incubation, the substrates were gently rinsed with Triton X-100 solution (0.1% v/v), then with ultrapure water (Milli Q®), and subsequently dried in air.

Triton X-100 effects on the thiolipid SAM. As a control for the electrochemical double layer capacitance measurements, some substrates were prepared as for the nAChR immobilization; however, the nAChR-containing solution was replaced with 0.1% v/v Triton X-100 aqueous solution.

Carb immobilization. The thiolipid–nAChR modified substrates were immersed for 30 min in a 0.5 mM Carb aqueous solution, gently rinsed with ultrapure water and dried in air.

AFM imaging

AFM imaging was carried out in air and in a liquid environment (0.1 mg ml^{-1} in 0.1% v/v Triton X-100 aqueous solution) with a Nanoscope V microscope from Bruker, operating in the tapping mode. Images were taken at a scanning rate of 1 Hz with etched silicon tips (RTESP, 215–254 kHz and 20–80 N m^{-1}) in air and with sharp silicon nitride tips (MSNL-10; 10 to 20 kHz and 0.01 to 0.06 N m^{-1}) in liquid.

AFM was also used to estimate the thiolipid SAM thickness by repetitive scanning of the sample with the AFM tip. To accomplish the removal of the thiolipid layer, the probe was swept multiple times across a small region with a high mechanical force (16 nN) applied to the AFM tip. This load was enough to open a window by removing the thiolipid molecules without damaging the underlying gold substrate. The sweeping action of the probe (k = 0.58 N m^{-1}) was used to remove or displace molecules of the matrix of the SAM. To achieve a high-quality removal of the thiol molecules, the sweeping was performed in ethanol media, a good solvent for thiolipid molecules, due to the fact that in air or water, most of the displaced molecules can remain partly attached to the gold surface. Then, the swept area was characterized using the same probe in a low force (0.08 nN) regime for nondestructive AFM imaging. The cross section analysis of the opened window allowed the estimation of the film thickness.

Electrochemical measurements

Electrochemical measurements were performed in a three-electrode electrochemical cell using a Teq galvanostat-potentiostat; the substrates prepared as described above were used as the working electrodes (counter electrode: platinum foil, reference electrode: saturated calomel electrode (SCE)). The electrolyte dissolution was 0.1 M NaOH, purged with N_2. Voltammograms were recorded at 0.1 V s^{-1}. Chronoamperometric measurements were carried out at −0.2 V *vs.* SCE with stirring of the electrolyte at 300 rpm. Carb was added at 3, 9 and 15 min by the addition of 1 mL of 30 mM Carb solution, reaching concentrations of 0.5 mM, 1.0 mM and 1.5 mM, respectively.

Thiolipid surface coverage (θ) on the Au surface was estimated by measuring the charge density (q) involved in the reductive desorption peak. The thiolipid reductive electrodesorption was performed by scanning the potential from −0.3 to −1.4 at 0.1 V s^{-1} in 0.1 M NaOH solution at room temperature. Then, the charge (Q_t) involved in the reductive peak desorption was calculated by integration of the peak area after subtraction of the charging current. On the other hand, the real electrode area was measured through the gold oxide reduction peak after the complete electrodesorption of thiolipid. The real surface area was then calculated as $A = Q/q_{mon}$, where Q is the charge involved in the Au oxide monolayer electroreduction and q_{mon} is the charge density related to the electroreduction of a gold oxide monolayer (q_{mon} = 440 μC cm^{-2}). Finally, the thiolipid charge density was obtained as $q = Q_t/A$. Considering the two electron transfer process for desorption of each thiolipid molecule, the θ value was estimated. The θ value

was also confirmed by comparing the q value with that obtained for the reductive desorption of hexanethiol (one electron per thiol molecule) adsorbed on the same substrate that yields q = 75 μC cm^{-2} for θ = 0.33. The results showed in this study were averaged for at least 6 voltammograms.

FTIR spectroscopy

FTIR spectra were acquired using a Varian 660 spectrometer equipped with an attenuated total reflection (ATR) accessory (MIRacle ATR, Pike Technologies) with a ZnSe prism or a diffused reflection accessory. Control spectra of the substrates obtained after each step of thiolipid and nAChR adsorption were carried out. In all cases, each spectrum was the result of 256 scans taken with a resolution of 2 cm^{-1}.

SPR measurements

SPR detection was carried out with a SPR-Navi 210A (Oy BioNavis Ltd, Tampere, Finland) instrument using gold sensor slides (Oy BioNavis Ltd, Tampere, Finland). Adsorption of thiolipid on a bare gold surface was measured in scanning angle mode with a SPR Navi™ 200 (BioNavis, Tampere, Finland) instrument using a 785 nm laser. SPR Navi™ Gold sensors (50 nm thickness of gold evaporated on glass slides) were cleaned with $NH_3:H_2O_2$ 1 : 1 solution prior to use. The ethanol flow rate was maintained at 10 μL min^{-1} and after a baseline was achieved, the thiolipid (0.1 mg mL^{-1} ethanolic solution) was injected at the same flow rate. The adsorption of the protein was carried out in a similar way by replacing the bare Au substrate with another, which had been previously immersed in the thiolipid solution for 24 h. Measurements were made in duplicate in parallel channels. The error in the measured values is 5%.

The surface coverage (Γ), including the instrument signal, was determined from the De Feijter equation[46] and can be expressed as:

$$\Gamma = \frac{\Delta\theta kd}{\mathrm{d}n/\mathrm{d}c} \quad (1)$$

where θ is the angular response in the measurement, k the instrument constant, d is the sample layer thickness and dn/dc is the refraction index concentration dependence. For the calculation, kd = 1.9 × 10^{-7} cm deg^{-1} was used for λ = 785 nm and dn/dc = 0.182 cm^3 g^{-1} and 0.135 cm^3 g^{-1} (ref. 47) were used for the protein and thiolipid.

Abbreviations

AFM	Atomic force microscopy
Carb	Carbamoylcholine
FTIR	Fourier transform infrared spectroscopy
nAChR	Nicotinic acetylcholine receptor
SAM	Thiolipid self-assembled monolayer
SPR	Surface plasmon resonance spectroscopy
TEM	Transmission electron microscopy
TM	Transmembrane domain

Acknowledgements

The authors acknowledge financial support from ANPCyT (PICT 2010-2554 to R. C. S., PICT 2010-1779 to P. L. S., PICT 2011-0604 to F. J. B.), Universidad Nacional de La Plata grant no. 11/X625 to P. L. S. and PIP no. 112-201101-01023 from the National Scientific and Technical Research Council of Argentina (CONICET) to F.J.B.

References

1 E. T. Castellana and P. S. Cremer, *Surf. Sci. Rep.*, 2006, **61**, 429–444.
2 X. Zhang, W. Fu, C. G. Palivan and W. Meier, *Sci. Rep.*, 2013, **3**, 2196.
3 R. P. Richter, J. L. K. Him and A. Brisson, *Mater. Today*, 2003, **6**, 32–37.
4 B. Schuster and U. B. Sleytr, *J. R. Soc. Interface*, 2014, **11**, 20140232.
5 S. K. Arya, P. R. Solanki, M. Datta and B. D. Malhotra, *Biosens. Bioelectron.*, 2009, **24**, 2810–2817.
6 H. Lang, C. Duschl and H. Vogel, *Langmuir*, 1994, **10**, 197–210.
7 S. Terrettaz, T. Stora, C. Duschl and H. Vogel, *Langmuir*, 1993, **9**, 1361–1369.
8 T. Stora, J. H. Lakey and H. Vogel, *Angew. Chem., Int. Ed.*, 1999, **38**, 389–392.
9 R. Naumann, S. M. Schiller, F. Giess, B. Grohe, K. B. Hartman, I. Kärcher, I. Köper, J. Lübben, K. Vasilev and W. Knoll, *Langmuir*, 2003, **19**, 5435–5443.
10 K. Tamada, M. Hara, H. Sasabe and W. Knoll, *Langmuir*, 1997, **13**, 1558–1566.
11 S. Terrettaz, W.-P. Ulrich, H. Vogel, Q. Hong, L. G. Dover and J. H. Lakey, *Protein Sci.*, 2002, **11**, 1917–1925.
12 D. A. Cisneros, D. J. Muller, S. M. Daud and J. H. Lakey, *Angew. Chem., Int. Ed.*, 2006, **45**, 3252–3256.
13 F. J. Barrantes, *Brain Res. Brain Res. Rev.*, 2004, **47**, 71–95.
14 K. Brejc, W. J. van Dijk, R. V. Klaassen, M. Schuurmans, J. van Der Oost, A. B. Smit and T. K. Sixma, *Nature*, 2001, **411**, 269–276.
15 F. J. Barrantes, *Curr. Opin. Drug Discovery Dev.*, 2003, **6**, 620–632.
16 F. J. Barrantes, *Biochim. Biophys. Acta, Biomembr.*, 2015, **1848**, 1796–1805.
17 Y. Xu, F. J. Barrantes, X. Luo, K. Chen, J. Shen and H. Jiang, *J. Am. Chem. Soc.*, 2005, **127**, 1291–1299.
18 X. Liu, Y. Xu, H. Li, X. Wang, H. Jiang and F. J. Barrantes, *PLoS Comput. Biol.*, 2008, **4**, 0100–0110.
19 N. Unwin, *Q. Rev. Biophys.*, 2013, **46**, 283–322.
20 H. Schindler, F. Spillecke and E. Neumann, *Proc. Natl. Acad. Sci. U. S. A.*, 1984, **81**, 6222–6226.
21 H. Schindler, J. P. Rosenbusch and U. Quast, *Neurochem. Int.*, 1980, **2C**, 291–298.
22 G. Boheim, W. Hanke, F. J. Barrantes, H. Eibl, B. Sakmann, G. Fels and A. Maelicke, *Proc. Natl. Acad. Sci. U. S. A.*, 1981, **78**, 3586–3590.

23 R. Lal and L. Yu, *Proc. Natl. Acad. Sci. U. S. A.*, 1993, **90**, 7280–7284.
24 N. Vuong, J. E. Baenziger and L. J. Johnston, *Chem. Phys. Lipids*, 2010, **163**, 117–126.
25 C. G. Clark, Z. Sun, G. a. Meininger and J. T. Potts, *Exp. Physiol.*, 2013, **98**, 415–424.
26 N. P. Barrera, H. Ge, R. M. Henderson, W. J. Fitzgerald and J. M. Edwardson, *Micron*, 2008, **39**, 101–110.
27 S. M. Schiller, R. Naumann, K. Lovejoy, H. Kunz and W. Knoll, *Angew. Chem., Int. Ed.*, 2003, **42**, 208–211.
28 T. Kakiuchi, H. Usui, D. Hobara and M. Yamamoto, *Langmuir*, 2002, **18**, 5231–5238.
29 D. Matyszewska, S. Sek and R. Bilewicz, *Langmuir*, 2012, **28**, 5182–5189.
30 T. Laredo, J. Leitch, M. Chen, I. J. Burgess, J. R. Dutcher and J. Lipkowski, *Langmuir*, 2007, **23**, 6205–6211.
31 Q. Zhang and L. A. Archer, *J. Phys. Chem. B*, 2003, **107**, 13123–13132.
32 R. G. Snyder, H. L. Strauss and C. A. Elliger, *J. Phys. Chem.*, 1982, **86**, 5145–5150.
33 D. L. Allara, A. N. Parikh and F. Rondelez, *Langmuir*, 1995, **11**, 2357–2360.
34 R. A. MacPhail, H. L. Strauss, R. G. Snyder and C. A. Elliger, *J. Phys. Chem.*, 1984, **88**, 334–341.
35 K. Kailasam, M. M. Natile, A. Glisenti and K. Müller, *J. Chromatogr., A*, 2009, **1216**, 2345–2354.
36 Y. Chang, W.-L. Chu, W.-Y. Chen, J. Zheng, L. Liu, R.-C. Ruaan and A. Higuchi, *J. Biomed. Mater. Res., Part A*, 2010, **93**, 400–408.
37 U. Gorne-Tschelnokow, A. Strecker, C. Kaduk, D. Naumann and F. Hucho, *EMBO J.*, 1994, **13**, 338–341.
38 H. Huang, L. Wang, Y. Cai, C. Zhou, Y. Yuan, X. Zhang, H. Wan and G. Guan, *CrystEngComm*, 2015, **17**, 1318–1325.
39 F. Barrantes, *J. Cell Biol.*, 1982, **92**, 60–68.
40 R. R. Kellner, C. J. Baier, K. I. Willig, S. W. Hell and F. J. Barrantes, *Neuroscience*, 2007, **144**, 135–143.
41 L. Becucci, M. D'Amico, S. Daniele, M. Olivotto, A. Pozzi and R. Guidelli, *Bioelectrochemistry*, 2010, **78**, 176–180.
42 A. Ciuraszkiewicz, W. Schreibmayer, D. Platzer, A. Orr-Urtreger, P. Scholze and S. Huck, *J. Physiol.*, 2013, **591**, 3271–3288.
43 I. K. Vockenroth, P. P. Atanasova, J. R. Long, A. T. A. Jenkins, W. Knoll and I. Köper, *Biochim. Biophys. Acta*, 2007, **1768**, 1114–1120.
44 L. Steller, M. Kreir and R. Salzer, *Anal. Bioanal. Chem.*, 2012, **402**, 209–230.
45 O. H. Lowry, N. J. Rosebrough, A. L. Farr and R. J. Randall, *J. Biol. Chem.*, 1951, **193**, 265–275.
46 J. A. De Feijter, J. Benjamins and F. A. Veer, *Biopolymers*, 1978, **17**, 1759–1772.
47 K. Hall, T.-H. Lee, A. I. Mechler, M. J. Swann and M.-I. Aguilar, *Sci. Rep.*, 2014, **4**, 5479.